Balanced Atmospheric Response to Squall Lines

WAYNE H. SCHUBERT

Department of Atmospheric Science, Colorado State University, Fort Collins, Colorado

SCOTT R. FULTON

Department of Mathematics and Computer Science, Clarkson University, Potsdam, New York

ROLF F. A. HERTENSTEIN

Department of Atmospheric Science, Colorado State University, Fort Collins, Colorado

19 August 1988 and 2 March 1989

ABSTRACT

When a squall line propagates through the atmosphere, it not only excites transient gravity–inertia wave motion but also produces more permanent modifications to the large-scale balanced flow. Here we calculate this balanced response using the isentropic/geostrophic coordinate version of semigeostrophic theory. This approach results in a simple mathematical form in which the horizontal ageostrophic velocities are completely implicit and the entire dynamics reduces to a predictive equation for the potential pseudodensity and an invertibility relation. For a two-dimensional squall line, the potential pseudodensity equation is simple enough to be solved analytically. The solutions illustrate how the squall line leaves in its wake a region of low potential pseudodensity in the lower troposphere and a region of high potential pseudodensity in the upper troposphere. The solutions also show that the character of the potential pseudodensity modification by the squall line depends on the ratio of the convective overturning time to the squall line passage time. This allows us to dynamically distinguish intensely raining, wide, slowly moving squall lines from weakly raining, narrow, fast-moving squall lines. After the potential pseudodensity is determined, it can be used in the invertibility relation to yield balanced wind and mass fields which capture some of the observed large-scale features associated with squall lines.

1. Introduction

A simple way to help understand the effects of moist convection on the large-scale atmospheric circulation is to incorporate these effects as apparent sources in the governing large-scale equations. If the apparent sources vary on time scales which are short compared to the geostrophic adjustment time, considerable transient gravity–inertia wave activity will result. However, what is more fundamental than these transient waves is the balanced response associated with the potential pseudodensity (the inverse of the potential vorticity) anomaly induced by the convection. This response is most easily studied in the context of a balanced model. Here we use semigeostrophic theory to study the balanced atmospheric response to a moving convective line. In section 2 we present three-dimensional semigeostrophic theory with diabatic effects. In section 3 we specialize this theory to the two-dimensional case, idealize a squall line as a moving midtropospheric heat source, solve the fundamental predictive equation analytically to obtain the potential pseudodensity anomaly induced by the squall line, and finally use multigrid methods to numerically solve the elliptic equation which relates the potential pseudodensity to the balanced wind and mass fields.

Corresponding author address: Dr. Wayne H. Schubert, Department of Atmospheric Science, Colorado State University, Fort Collins, CO 80523.

2. Semigeostrophic theory

Let us first review what is apparently the most elegant and concise version of semigeostrophic theory—that version which makes simultaneous use of geostrophic and isentropic coordinates. With these coordinates, semigeostrophic theory reduces to two equations—a predictive equation for the potential pseudodensity [see (2.11) below] and a diagnostic equation or invertibility principle [see (2.14) below] whose solution yields the balanced wind and mass fields from the potential pseudodensity.

We begin with the frictionless, f-plane system of equations with the geostrophic momentum approximation (Hoskins 1975). Using potential temperature as the vertical coordinate, our system becomes

$$\frac{Du_g}{Dt} - fv_a = 0, \tag{2.1}$$

$$\frac{Dv_g}{Dt} + fu_a = 0, \tag{2.2}$$

$$\frac{\partial M}{\partial \theta} = \Pi, \tag{2.3}$$

$$\frac{D\sigma}{Dt} + \sigma\left(\frac{\partial u}{\partial x} + \frac{\partial v}{\partial y} + \frac{\partial \dot{\theta}}{\partial \theta}\right) = 0, \tag{2.4}$$

where $(u_g, v_g) = f^{-1}(-\partial M/\partial y, \partial M/\partial x)$ are the components of geostrophic velocity, (u, v) the horizontal components of the total velocity, $(u_a, v_a) = (u - u_g, v - v_g)$ the components of the ageostrophic velocity, $\Pi = c_p(p/p_0)^\kappa$ the Exner function, $M = \theta\Pi + \phi$ the Montgomery potential, $\sigma = -\partial p/\partial\theta$ the pseudodensity, and $D/Dt = \partial/\partial t + u\partial/\partial x + v\partial/\partial y + \dot{\theta}\partial/\partial\theta$ the total derivative.

The equation for the absolute *isentropic* vorticity can be derived from (2.1) and (2.2). It can be written in the form

$$\frac{\partial(\sigma P)}{\partial t} + \frac{\partial(u\sigma P - \dot{\theta}\xi)}{\partial x} + \frac{\partial(v\sigma P - \dot{\theta}\eta)}{\partial y} = 0, \tag{2.5}$$

where $P = \zeta/\sigma$ is the potential vorticity and where

$$(\xi, \eta, \zeta) = f\left(\frac{\partial(X,Y)}{\partial(y,\theta)}, \frac{\partial(X,Y)}{\partial(\theta,x)}, \frac{\partial(X,Y)}{\partial(x,y)}\right), \tag{2.6}$$

with X and Y defined below in (2.8). The significance of (2.5) has recently been discussed by Haynes and McIntyre (1987), who draw attention to the fact that in the isentropic coordinate a flux form such as (2.5) leads directly to the theorem that even with diabatic heating "there can be no net transport of potential vorticity across any isentropic surface" and that "potential vorticity can neither be created nor destroyed within a layer bounded by two isentropic surfaces." In this sense, an isentropic surface is "impermeable to potential vorticity," and "the potential vorticity in a layer between two isentropic surfaces is indestructible" as long as the layer does not meet a boundary such as the earth's surface. The above arguments also apply when friction is included.

We can now combine (2.4) and (2.5) to obtain

$$\frac{D\sigma^*}{Dt} + \frac{\sigma^*}{\zeta}\left(\xi\frac{\partial}{\partial x} + \eta\frac{\partial}{\partial y} + \zeta\frac{\partial}{\partial\theta}\right)\dot{\theta} = 0, \tag{2.7}$$

where $\sigma^* = (f/\zeta)\sigma$ is the potential pseudodensity. We can interpret σ^* as the pseudodensity the fluid element would acquire if ζ were changed to f under a frictionless and adiabatic rearrangement process. As we shall see from the simplicity of (2.11), σ^* seems to be a more convenient variable than its inverse, the more commonly used potential vorticity.

The duality between the use of geostrophic coordinates in the horizontal and the isentropic coordinate in the vertical has been discussed by Hoskins and Draghici (1977). The combined use of geostrophic and isentropic coordinates has been discussed theoretically by McWilliams and Gent (1980) and has found application in the two-dimensional upper tropospheric frontogenesis study of Buzzi et al. (1981). Here we are concerned with the simultaneous use of geostrophic and isentropic coordinates because it will lead to an elegant version of the potential pseudodensity equation. Thus, introducing the geostrophic coordinates

$$(X, Y, \Theta, T) = (x + v_g/f, y - u_g/f, \theta, t), \tag{2.8}$$

we can easily show that

$$\zeta\frac{\partial}{\partial\Theta} = \xi\frac{\partial}{\partial x} + \eta\frac{\partial}{\partial y} + \zeta\frac{\partial}{\partial\theta}, \tag{2.9}$$

$$\frac{D}{Dt} = \frac{\partial}{\partial T} + u_g\frac{\partial}{\partial X} + v_g\frac{\partial}{\partial Y} + \dot{\theta}\frac{\partial}{\partial\Theta}, \tag{2.10}$$

which lead to a considerable simplification of (2.7). Specifically, we can now write the potential pseudodensity equation (2.7) as

$$\frac{\partial\sigma^*}{\partial T} + \frac{\partial(u_g\sigma^*)}{\partial X} + \frac{\partial(v_g\sigma^*)}{\partial Y} + \frac{\partial(\dot{\theta}\sigma^*)}{\partial\Theta} = 0, \tag{2.11}$$

which serves as the fundamental predictive equation of the model. A major advantage of the transformation from (x, y, θ, t) space to (X, Y, Θ, T) space is the change from advection by (u, v) to advection by (u_g, v_g).

In order to express the geostrophic and hydrostatic equations in (X, Y, Θ, T) space, it is convenient to introduce the Bernoulli function $M^* = M + (u_g^2 + v_g^2)/2$. Then, it can be shown that the geostrophic and hydrostatic relations in (X, Y, Θ, T) take the form

$$(fv_g, -fu_g, \Pi) = \left(\frac{\partial M^*}{\partial X}, \frac{\partial M^*}{\partial Y}, \frac{\partial M^*}{\partial\Theta}\right), \tag{2.12}$$

which is identical to the form taken in (x, y, θ, t).

The potential pseudodensity σ^* is a combination of the mass field σ and the wind field ζ. However, since σ is related to M^* through hydrostatic balance and ζ is related to M^* through geostrophic balance, σ^* depends only on M^*. Thus, everything can be obtained from σ^* if we can somehow invert it to obtain M^*. The relation between M^* and σ^* is derived as follows. From the definition of σ^* we have

$$\frac{\partial(x, y, \Pi)}{\partial(X, Y, \Theta)} + \Gamma\sigma^* = 0 \tag{2.13}$$

where $\Gamma = d\Pi/dp = \kappa\Pi/p$. Expressing x and y in terms of u_g and v_g by (2.8), and then using (2.12), we can write (2.13) as

$$\left(f^2 - \frac{\partial^2 M^*}{\partial X^2}\right)\left(\frac{\partial^2 M^*}{\partial Y\partial\Theta}\right)^2 + \left(f^2 - \frac{\partial^2 M^*}{\partial Y^2}\right)\left(\frac{\partial^2 M^*}{\partial X\partial\Theta}\right)^2 + 2\left(\frac{\partial^2 M^*}{\partial X\partial Y}\right)\left(\frac{\partial^2 M^*}{\partial Y\partial\Theta}\right)\left(\frac{\partial^2 M^*}{\partial\Theta\partial X}\right)$$

$$+\left\{f^2\left(f^2-\frac{\partial^2 M^*}{\partial X^2}-\frac{\partial^2 M^*}{\partial Y^2}\right)+\left(\frac{\partial^2 M^*}{\partial X^2}\right)\left(\frac{\partial^2 M^*}{\partial Y^2}\right)-\left(\frac{\partial^2 M^*}{\partial X \partial Y}\right)^2\right\}\frac{\partial^2 M^*}{\partial \Theta^2}+f^4\Gamma\sigma^*=0. \quad (2.14a)$$

If the upper boundary is an isentropic and isobaric surface with potential temperature Θ_T and Exner function Π_T, the upper boundary condition for (2.14a) is simply

$$\frac{\partial M^*}{\partial \Theta}=\Pi_T \quad \text{at} \quad \Theta=\Theta_T. \quad (2.14b)$$

If we neglect the effects of topography and assume that the lower boundary is the constant height surface $\phi = 0$ and the isentropic surface $\Theta = \Theta_B$, then $M = \Theta\Pi$ at $\Theta = \Theta_B$. Written in terms of M^*, this lower boundary condition becomes

$$M^*-\Theta\frac{\partial M^*}{\partial \Theta}-\frac{1}{2f^2}\left[\left(\frac{\partial M^*}{\partial X}\right)^2+\left(\frac{\partial M^*}{\partial Y}\right)^2\right]=0 \quad \text{at} \quad \Theta=\Theta_B. \quad (2.14c)$$

The lateral boundary conditions depend on the particular application.

Equations (2.11), (2.12) and (2.14) form a closed system. The computational scheme is to solve (2.14) for M^*, use (2.12) to compute u_g and v_g, and then use (2.11) to predict a new σ^*. Note that the combined use of isentropic and geostrophic coordinates has resulted in the disappearance of all divergent, ageostrophic components from the fundamental predictive relation (2.11). We have used a related coordinate transformation and more general balance condition to study the evolution of potential vorticity and wind in tropical cyclones (Schubert and Alworth 1987). The underlying theoretical structure is the same—a predictive equation for σ^* and an invertibility relation for obtaining M^* from σ^*. The success of this general approach suggests that it may be the simplest way of looking at all types of balanced flows—whether they be adiabatic, frictionless baroclinic waves of the midlatitude troposphere, breaking planetary waves of the stratosphere or thermally forced tropical systems.

3. Atmospheric response to a moving squall line

Let us now consider an infinitely long squall line which induces a two-dimensional flow with $\partial/\partial y = \partial/\partial Y = 0$, $u = u_a$ (i.e., $u_g = 0$) and $v = v_g$ (i.e., $v_a = 0$). Equation (2.11) then reduces to

$$\frac{\partial \sigma^*}{\partial T}+\frac{\partial}{\partial \Theta}(\dot{\theta}\sigma^*)=0, \quad (3.1)$$

and (2.14) to

$$\left(f^2-\frac{\partial^2 M^*}{\partial X^2}\right)\frac{\partial^2 M^*}{\partial \Theta^2}+\left(\frac{\partial^2 M^*}{\partial X \partial \Theta}\right)^2+f^2\Gamma\sigma^*=0, \quad (3.2a)$$

$$\frac{\partial M^*}{\partial \Theta}=\Pi_T \quad \text{at} \quad \Theta=\Theta_T, \quad (3.2b)$$

$$M^*-\Theta\frac{\partial M^*}{\partial \Theta}-\frac{1}{2f^2}\left(\frac{\partial M^*}{\partial X}\right)^2=0 \quad \text{at} \quad \Theta=\Theta_B. \quad (3.2c)$$

Because the geostrophic flow does not advect σ^* in the two-dimensional case, we can now solve (3.1) for σ^* independent of the solution of (3.2).

Let us consider a heat source with a Gaussian shape in X and a midtropospheric maximum. This source is assumed to be switched on at time $T = 0$ and to propagate eastward at constant speed c_0, so that

$$\dot{\theta}=Q_0\exp\left[-\frac{(X-c_0T)^2}{X_0^2}\right]\sin\left[\frac{\pi(\Theta-\Theta_B)}{\Theta_T-\Theta_B}\right] \quad (3.3)$$

for $T > 0$, where Q_0 is the magnitude and X_0 the e-folding half-width of the heat source. Substituting (3.3) in (3.1) we obtain

$$\alpha e^{\tau^2}\frac{\partial}{\partial \tau}(\sigma^*\sin Z)+\sin Z\frac{\partial}{\partial Z}(\sigma^*\sin Z)=0, \quad (3.4)$$

where $Z = \pi(\Theta - \Theta_B)/(\Theta_T - \Theta_B)$ and $\tau = (c_0T - X)/X_0$. The dimensionless parameter

$$\alpha=\frac{(\Theta_T-\Theta_B)/(\pi Q_0)}{X_0/c_0}$$

can be regarded as the ratio of the convective overturning time to the squall line passage time. Thus, α is small for intensely raining, wide, slowly moving squall lines while it is large for weakly raining, narrow, fast moving squall lines. The two case studies of Oklahoma squall lines by Ogura and Chen (1977) and Ogura and Liou (1980) indicate that for a typical squall line $\Theta_T - \Theta_B = 40$ K, $Q_0 = 7$ K h^{-1}, $X_0 = 40$ km and $c_0 = 50$ km h^{-1} so that $\alpha = 2.3$.

According to (3.4) the quantity $\sigma^* \sin Z$ is constant along each characteristic curve determined from $d\tau/(\alpha e^{\tau^2}) = dZ/(\sin Z)$. By integration of this characteristic equation we can show that the characteristic through the point (X, Z, T) approaches (in the far field) the level

$$Z_0(X, Z, T)=2\tan^{-1}\left(e^{-\beta(X,T)}\tan\frac{Z}{2}\right), \quad (3.5)$$

where

$$\beta(X, T)=\frac{\sqrt{\pi}}{2\alpha}\left[\operatorname{erf}\left(\frac{c_0T-X}{X_0}\right)+\operatorname{erf}\left(\frac{X}{X_0}\right)\right]. \quad (3.6)$$

Let us assume that as $X \to \pm\infty$, σ^* approaches the constant σ_0. Since $\sigma^* \sin Z$ is constant along each characteristic, we can write the solution of (3.1) as

$$\sigma^*(X, Z, T)=\sigma_0\frac{\sin Z_0(X, Z, T)}{\sin Z}. \quad (3.7a)$$

Although (3.7a) is indeterminate at the top and bottom boundaries, use of L'Hopital's rule yields

$$\sigma^*(X, Z, T) = \sigma_0 \begin{cases} e^{\beta(X,T)} & Z = \pi \\ e^{-\beta(X,T)} & Z = 0. \end{cases} \quad (3.7b)$$

In summary, (3.7) along with the auxiliary relations (3.5) and (3.6) give the analytic solution of (3.1) with the specified heating (3.3). Figures 1a and 2a show σ_0/σ^* computed from (3.7) for the case $\alpha = 2.3$ for both $T = 8$ and $T = 16$ h. The squall line, which started at $X = 0$, has left in its wake a region of high potential vorticity in the lower troposphere and a region of low potential vorticity in the upper troposphere. A comparison of Figs. 1a and 2a shows that the potential vorticity anomaly has not increased in magnitude but has increased in horizontal extent as the squall line has propagated along the domain.

Our final task is to invert this σ^* field to obtain the associated balanced wind and mass fields. To accomplish this we first isolate the dynamically significant portion of M^* by subtracting out a horizontally uniform basic state, i.e., $\mathcal{M} = M^* - \bar{M}^*$. The basic state field corresponds to the solution of (3.2) when the potential pseudodensity is the constant σ_0. Lateral boundary conditions are obtained by noting that if $\sigma^* \to \sigma_0$ as $X \to \pm\infty$ and if the far-field solution is horizontally homogeneous, then $M^* \to \bar{M}^*$ as $X \to \pm\infty$. Thus we use the Dirichlet lateral boundary condition $\mathcal{M} = 0$, placing the lateral boundaries far enough out that their influence on the solution is minimal. For the numerical solution we discretize on a uniform grid using second-order centered differences and ghost points to allow centered differencing in the

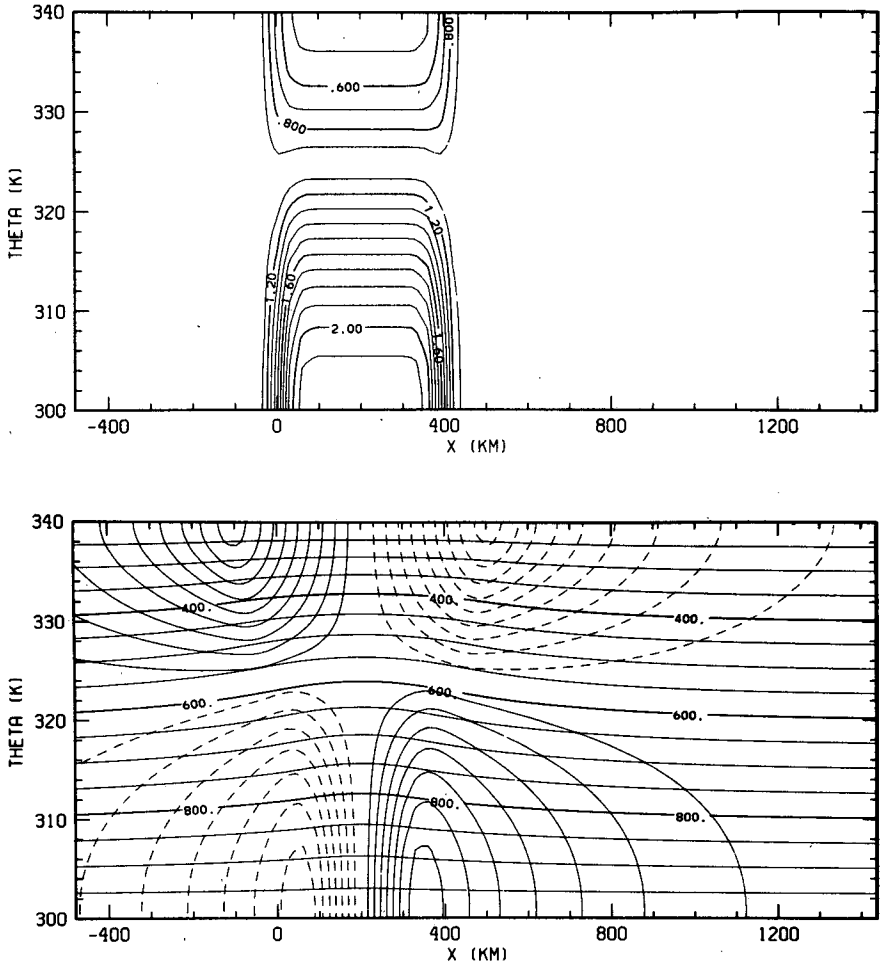

FIG. 1. Results for $T = 8$ h and $\alpha = 2.3$. (a) Isolines of σ_0/σ^* (i.e., potential vorticity measured in units of f) in (X, Θ) space. Note that the passage of the squall line generates a lower tropospheric layer of high potential vorticity and an upper tropospheric layer of low potential vorticity. (b) Pressure (nearly horizontal lines) in millibars and geostrophic wind along the squall line in m s^{-1}. Solid wind contours indicate flow into the page, dashed contours flow out of the page. The contour interval for the winds is 1 m s^{-1} with the zero line omitted. These wind and mass fields are in (x, θ) space and are associated with the potential vorticity field shown in (a). The geostrophic wind maxima coincide with the location of the largest horizontal gradient of potential vorticity.

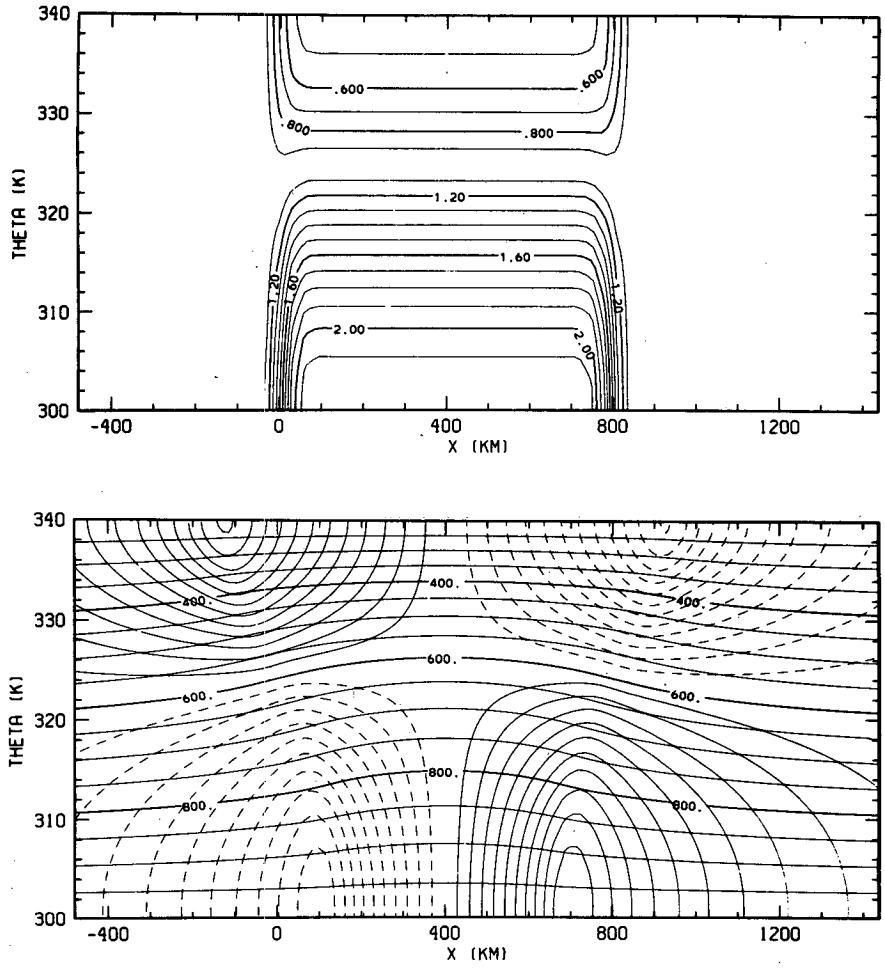

FIG. 2. As in Fig. 1, but for $T = 16$ h.

vertical boundary conditions. The resulting discrete system is solved efficiently by a multigrid method, a detailed description of which is given in Fulton (1989). For the results shown here we have used a computational domain which extends vertically from $\Theta = 300$ to 340 K and horizontally from $X = -1437$ to 4311 km (a horizontal domain size of six Rossby lengths). This domain has been divided into 32 grid intervals in the vertical and 192 intervals in the horizontal. The resulting balanced fields in (x, θ) space are shown in the remainder of Figs. 1 and 2. Because of the simple far-field decay of the balanced components, only a central region (-479 km $< x <$ 1437 km) of the computational domain has been displayed. In the lower tropospheric region swept out by the squall line, the positive potential vorticity anomaly causes cyclonic shear with positive v_g at the current squall line position and negative v_g at the start-up position. In those lower tropospheric regions where the potential vorticity is unmodified, the horizontal wind shear is anticyclonic. In the upper troposphere the flow field is reversed because the negative potential vorticity anomaly causes anticyclonic shear. At $T = 8$ h a maximum geostrophic flow of 7 m s^{-1} at lower levels and 9 m s^{-1} at upper levels has been produced by the squall line. By $T = 16$ h the squall line has propagated over nearly one Rossby length so that less cancellation occurs between the flows induced by the two edges of the potential vorticity anomaly. Accordingly, the maximum lower and upper level geostrophic flows have increased to 10 and 12 m s^{-1}, respectively. Figures 1 and 2 also show the distortion of the pressure field due to the squall line. Behind the squall line there has been a decrease in σ (stabilization) in the lower troposphere and an increase in σ (destabilization) in the upper troposphere. This is simply a reflection of the mutual adjustment of the wind and mass fields. This adjustment occurs in such a way that in the lower troposphere where $P = \zeta/\sigma$ is large, ζ is large and σ is small, while in the upper troposphere where P is small, ζ is small and σ is large. This dynamical adjustment of the upper tropospheric static stability may play a role in the maintenance of the stratiform rain region that is often observed in the wake of both tropical and midlatitude squall lines. The region of

maximum upper tropospheric destabilization in Figs. 1 and 2 is displaced behind the squall line; observationally, this is in rough agreement with the relative position of regions of maximum upper level stratiform activity. Thus, it is possible that the upper level destabilization does produce a favorable background state for this mesoscale feature.

4. Concluding remarks

Although the model presented here does not capture the complicated moist physics associated with the convective and stratiform regions, it does predict some of the observed features of squall lines. Potential vorticity anomalies with roughly similar patterns to those predicted by the model have been observed for midlatitude squall lines (Hertenstein 1988). However, the observed potential vorticity anomalies appear to have considerably more structural detail than those produced by the model.

Although we have limited our attention to the case where the earth's surface is also an isentropic surface, certain aspects of squall lines require a more general view. For example, low-level evaporative cooling due to falling rain can be considered to locally draw up isentropic surfaces which were just under the ground. When an isentropic surface intersects the earth's surface, we can regard it as continuing just under the earth's surface with a pressure equal to the surface pressure. At any horizontal position where two distinct isentropic surfaces run just under the earth's surface (and hence have the same pressure), there is no mass trapped between them, so that $\sigma^* = \sigma = 0$ there. We can regard the Θ_B in (2.14c) as the largest value of Θ which remains everywhere below the earth's surface. Thus, we can use (2.11) to predict σ^* and (2.14) to diagnose M^* on all Θ surfaces such that $\Theta > \Theta_B$. The latter half of this procedure has been elegantly illustrated by Hoskins et al. (1985) and is consistent with Bretherton's (1966) conclusion that "any flow with potential temperature variations over a horizontal rigid plane boundary may be considered equivalent to a flow without such variations, but with a concentration of potential vorticity very close to the boundary." Of course, such a procedure has implications for the numerical methods used to solve (2.11) and (2.14) since we must cope with sharp gradients of σ^* and must guarantee that σ^* is positive definite.

Finally, it may be of interest to compare the invertibility relation discussed here [i.e., (2.14) or (3.2)] with that discussed by Hoskins et al. [1985, Eq. (29)]. Both use isentropic coordinates in the vertical but Hoskins et al. use the physical coordinate in the horizontal rather than the geostrophic coordinate. The use of physical coordinates in the invertibility relation presents no problem but their use in the potential pseudodensity equation means that ageostrophic advection must be explicitly handled. Thus, physical coordinates may be useful in diagnostic studies, but for a closed, predictive theory the horizontal coordinate used in the invertibility relation must be matched to the convenient coordinate used for the prediction of σ^*. A second difference between these two studies involves the "order" of the invertibility relation. The invertibility relation of Hoskins et al. is a second order partial differential equation for the rotational wind rather than for M^*, so that the forcing is the horizontal derivative of the potential vorticity rather than the potential vorticity itself. In this sense, the invertibility condition of Hoskins et al. is of a higher differential order. The apparent consequence of this fact is that Hoskins et al. are careful to include some kind of reference state which expresses the mass distribution of θ and, in order to eliminate arbitrariness, to speak of inversion relative to this or that reference state. In our approach it is not necessary to explicitly refer to a reference state in order to obtain uniqueness. A uniqueness proof for the solutions of (3.2) follows closely the arguments given in appendix A of Schubert and Alworth (1987).

Acknowledgments. This research was funded by NSF Grants ATM 8618079 and 8814541 and by ONR Grant N00014-87-K-0535.

REFERENCES

Bretherton, F. P., 1966: Critical layer instability in baroclinic flows. *Quart. J. R. Met. Soc.*, **92,** 325–334.

Buzzi, A., A. Trevisan and G. Salustri, 1981: Internal frontogenesis: A two-dimensional model in isentropic, semigeostrophic coordinates. *Mon. Wea. Rev.*, **109,** 1053–1060.

Fulton, S. R., 1989: Multigrid solution of the semigeostrophic invertibility relation. *Mon. Wea. Rev.*, **117,** (9), in press.

Haynes, P. H., and M. E. McIntyre, 1987: On the evolution of vorticity and potential vorticity in the presence of diabatic heating and frictional or other forces. *J. Atmos. Sci.*, **44,** 828–841.

Hertenstein, R. F. A., 1988: Modeling and observations of the atmospheric response to squall lines. Department of Atmospheric Science Rep. No. 434, Colorado State University, Fort Collins, CO, 96 pp.

Hoskins, B. J., 1975: The geostrophic momentum approximation and the semigeostrophic equations. *J. Atmos. Sci.*, **32,** 233–242.

——, and I. Draghici, 1977: The forcing of ageostrophic motion according to the semigeostrophic equations and in an isentropic coordinate model. *J. Atmos. Sci.*, **34,** 1859–1867.

——, M. E. McIntyre and A. W. Robertson, 1985: On the use and significance of isentropic potential vorticity maps. *Quart. J. R. Met. Soc.*, **111,** 877–946.

McWilliams, J. C., and P. R. Gent, 1980: Intermediate models of planetary circulations in the atmosphere and ocean. *J. Atmos. Sci.*, **37,** 1657–1678.

Ogura, Y., and Y.-L. Chen, 1977: A life history of an intense mesoscale convective storm in Oklahoma. *J. Atmos. Sci.*, **34,** 1458–1476.

——, and M.-T. Liou, 1980: The structure of a midlatitude squall line: A case study. *J. Atmos. Sci.*, **37,** 553–567.

Schubert, W. H., and B. T. Alworth, 1987: Evolution of potential vorticity in tropical cyclones. *Quart. J. R. Met. Soc.*, **113,** 147–162.